XII International Conference on Computational Plasticity. Fundamentals and Applications
COMPLAS XII
E. Oñate, D.R.J. Owen, D. Peric and B. Suárez (Eds)

# NUMERICAL SIMULATIONS OF SUBMERGED AND PRESSURISED X65 STEEL PIPES – COMPLAS XII

**MARTIN KRISTOFFERSEN*, FOLCO CASADEI†, TORE BØRVIK*, MAGNUS LANGSETH*, GEORGE SOLOMOS† AND ODD STURE HOPPERSTAD***

* Structural Impact Laboratory (SIMLab), Centre for Research-based Innovation (CRI)
Department of Structural Engineering, Norwegian University of Science and Technology
Rich. Birkelands vei 1a, NO-7491 Trondheim, Norway
e-mail: ikt-admin@ivt.ntnu.no – web page: http://www.ntnu.edu/simlab/

† European Laboratory for Structural Assessment (ELSA)
Institute for the Protection and Security of the Citizen (ISPC), Joint Research Centre (JRC)
21027 Ispra, Italy
e-mail: ipsc@jrc.it – web page: http://elsa.jrc.ec.europa.eu

**Key words:** Computational Plasticity, Fluid-structure Interaction, Impact Load

**Abstract.** While in service, pipelines may from time to time be exposed to impact loads from anchors or trawl gear. A lot of parameters influence the behaviour of the pipeline during impact, e.g. the diameter and thickness of the pipeline, the impactor's mass and velocity, and of course the material used. Also potentially influencing the deformation pattern is the presence of surrounding water, which can be a difficult parameter to include experimentally. The pressurised contents of the pipeline can also be an influencing factor. To gain some insight into how the water and possible pressure inside the pipeline affect the global impact behaviour, numerical investigations have been carried out using FSI-techniques available in the explicit finite element code Europlexus. One case was set up for validation against available experimental data, and additional cases examined numerically the effect of including pressure and/or surrounding water. The simulations generally captured the deformation and load levels from the experiments well, and may be assumed to represent the events with reasonable accuracy. Adding internal pressure generally led to a higher peak load, and created a more localised deformation. Submerging the pipe in water seemed to be of minor importance with respect to global and local deformation, but this depended heavily on the FSI conditions. Other parameters than the surrounding water, which for design purposes may be omitted, appear to be more significant to the global and local response.

# 1 INTRODUCTION

Transportation of oil and gas is a crucial part of the offshore industry. To this end, pipelines are under widespread use, often under high pressures and temperatures [1]. Impacts from trawl gear and anchors are known to cause problems, see e.g. [2]. Occurences like these necessitate assessments regarding the hazards and potential damage arising from such events [3], as failure in a pipeline transporting oil and/or gas could result in severe environmental and economic damage.

Det Norske Veritas (DNV) has published a standard on general design of pipeline systems [4] and specified some recommended practice on interference between pipelines and trawl gear [5]. The latter of these provides a simplified analysis for pipeline design, while allowing for use of numerical analyses and model tests in the design phase. The open literature provides several studies on pipeline impact. Thomas et al. [6] did impact tests where a wedge was dropped onto the midspan of a simply supported pipe, and compared them to quasi-static tests. Fully clamped pipes have been studied by Jones et al. [7]. Pressurised pipes have been investigated in [8, 9] and more recently in [10], while impact against submerged pipes seems to have been hardly studied at all.

This study presents a numerical investigation of impact against a simply supported pipe in four main conditions – in air and in water, with and without internal pressure. In [11], a pendulum accelerator was used to launch a trolley with a given mass and velocity against a simply supported pipe. No surrounding water was present and no internal pressure was applied to the pipe, and this case serves as a validation case for the simulations. On a global level, adding pressure seemed to give a higher peak load and more localised deformation, while submerging the pipe seemed to have little or no effect on the overall response at the relatively low impact velocities considered in this study.

# 2 PIPELINE MATERIAL

## 2.1 About the pipeline material

The pipeline material is an X65 grade offshore steel, a material widely used in pipelines conveying oil and/or gas [12]. According to the material inspection certificate, the yield strength is 450 MPa and the ultimate tensile strength is 535 MPa. Young's modulus is 208000 MPa. The pipes used are made seamless by utilising the Mannesmann effect, and are supplied by Tenaris, Argentina.

## 2.2 Material tests

Quasi-static material tests investigating the homogeneity and anisotropy of this material have been carried out in [11], and are succinctly summarised here. Specimens of geometry as shown in Fig. 1 were loaded to failure in tension at quasi-static strain rate and at room temperature. By using a laser-based measuring device, the minimum diameter was recorded continuously during testing and true stress-true strain curves, shown in Fig. 2(a) and (b), were obtained.

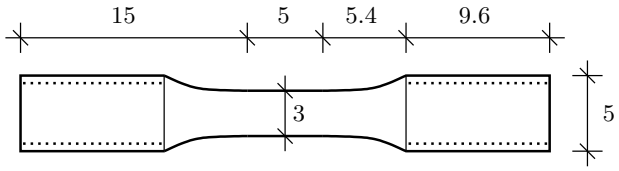


**Figure 1**: Specimen geometry for quasi-static tensile tests. Dimensions in mm.

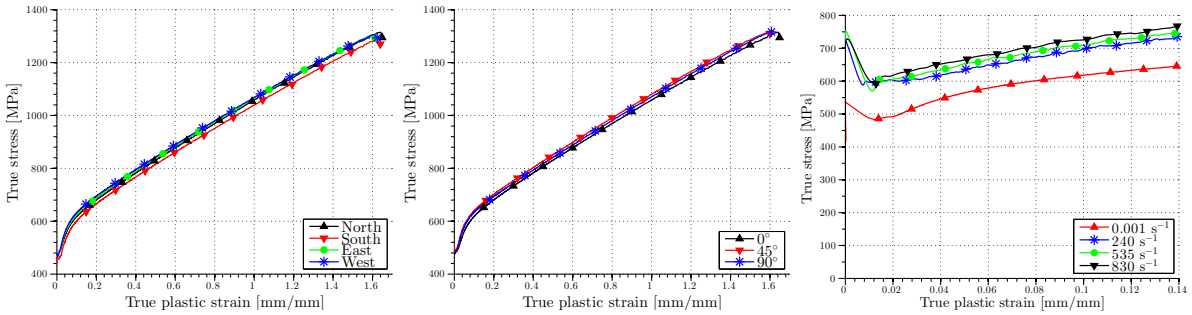


(a) Section homogeneity (b) Anisotropy (c) Rate dependency

**Figure 2**: Data from tensile tests on uniaxial specimens.

For engineering and design purposes, the material appears to be both homogeneous and isotropic. Based on values from 12 tests, the material yields at $478 \pm 15$ MPa and has a nominal peak stress of $572 \pm 14$ MPa. It strain hardens to a true peak stress of $1314 \pm 12$ MPa and fails at a true strain of $1.61 \pm 0.03$ by a ductile cup-and-cone fracture.

In addition, dynamic tensile tests on the same specimen geometry were conducted in a split Hopkinson tension bar [13], the workings of which are described in [14]. An increase of flow stress is observed with increasing strain rate, a common property of many metals. This is typically accompanied by an equivalent decrease of fracture strain, albeit not in this case. While the flow stress increased by about 20% (see Fig. 2(c)), the fracture strain $\varepsilon_f$ – as calculated by $\varepsilon_f = \ln(A_0/A_f)$ where $A_0$ is the initial cross-sectional area and $A_f$ is the cross-sectional area at fracture – remained of the same order as for the quasi-static tests (less than 1% alteration and within the standard deviation from the quasi-static tests).

## 2.3 Material model

To model the X65 material, the Johnson-Cook (JC) constitutive relation [15] has been used. It accounts for isotropic hardening, strain rate dependency and thermal effects. A von Mises yield criterion is used with an associated flow rule. The von Mises equivalent stress $\sigma_{eq}$ is a function of the deviatoric part $\boldsymbol{\sigma}^{\text{dev}}$ of the Cauchy stress tensor $\boldsymbol{\sigma}$,

$$\sigma_{eq}(\boldsymbol{\sigma}) = \sqrt{\frac{3}{2}\,\boldsymbol{\sigma}^{\text{dev}} : \boldsymbol{\sigma}^{\text{dev}}} \tag{1}$$

The JC flow stress $\sigma_{JC}$ is expressed as

$$\sigma_{JC}\left(\varepsilon_{eq}, \dot{\varepsilon}^*_{eq}, T^*\right) = \left(A + B\varepsilon^n_{eq}\right)\left(1 + C\ln\dot{\varepsilon}^*_{eq}\right)\left(1 - T^{*m}\right) \tag{2}$$

where $\varepsilon_{eq}$ is the equivalent plastic strain, and $A$, $B$, $n$, $C$ and $m$ are material constants. The dimensionless plastic strain rate is given by $\dot{\varepsilon}^*_{eq} = \dot{\varepsilon}_{eq}/\dot{\varepsilon}_0$, where $\dot{\varepsilon}_0$ is a user-defined reference strain rate, which is thought to be the minimum plastic strain rate for which material tests have been done. Strain rates below this threshold are treated as static.

The homologous temperature is defined as $T^* = (T - T_r)/(T_m - T_r)$, where $T$ is the absolute temperature, $T_r$ is the ambient temperature and $T_m$ is the melting temperature of the material. This problem is assumed to be isothermal, thus omitting the temperature bracket of Eq. (2) and thereby reducing it to

$$\sigma_{JC}\left(\varepsilon_{eq}, \dot{\varepsilon}_{eq}\right) = \left(A + B\varepsilon^n_{eq}\right)\left(1 + C\ln\frac{\dot{\varepsilon}_{eq}}{\dot{\varepsilon}_0}\right) \tag{3}$$

Then, from Eq. (1) and Eq. (3), the dynamic yield function $f_{JC}$ becomes

$$f_{JC}\left(\boldsymbol{\sigma}, \varepsilon_{eq}, \dot{\varepsilon}_{eq}\right) = \sigma_{eq}\left(\boldsymbol{\sigma}\right) - \sigma_{JC}\left(\varepsilon_{eq}, \dot{\varepsilon}_{eq}\right) \tag{4}$$

The initial size of the yield surface, i.e. when the equivalent plastic strain is zero, is given by the constant $A$. Implementation of the model is described in [16], and the material constants for the JC model are the same as used in [13]. No failure criterion has been used in this study.

### 2.4 Identification of material constants

To determine the equivalent stress $\sigma_{eq}$ from the measured major principal stress $\sigma_1$ after necking, Bridgman's analysis [17] was employed

$$\sigma_{eq} = \frac{\sigma_1}{\left(1 + \frac{2R}{a}\right) \cdot \ln\left(1 + \frac{a}{2R}\right)} \tag{5}$$

The relation between the radius of the specimen's cross-section at the root of the neck, $a$, and the radius of the neck profile, $R$, was estimated by the empirical relation proposed by Le Roy et al. [18]

$$\frac{a}{R} = 1.1 \cdot \left(\varepsilon_{eq} - \varepsilon_U\right) \tag{6}$$

valid for $\varepsilon_{eq} > \varepsilon_U$ where $\varepsilon_U$ is the equivalent plastic strain at the onset of necking. Material data from Fig. 2 was then used to calibrate the JC model in Eq. (3). Fracture was not accounted for in this study as the global response was the main topic of interest. All constants used in this study and details on the calibration can be found in [19].

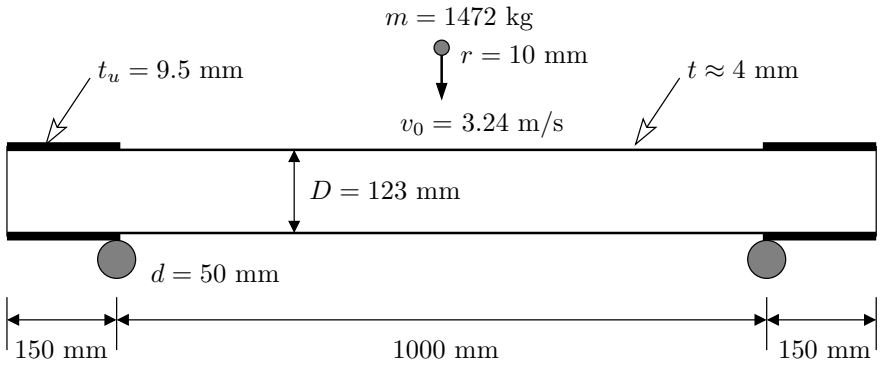


**Figure 3**: General setup of impact test against an X65 pipe.

## 3 COMPONENT TESTS

The component test used for validation of the numerical model is pipe A from the impact experiments carried out by Kristoffersen et al. [11]. A trolley weighing 1472 kg with a rigid nose of radius 10 mm impacts a simply supported pipe at an initial velocity of 3.24 m/s in a pendulum accelerator [20]. The pipe has an inner diameter of 123 mm and a thickness of about 4 mm after being lathed down from 9.5 mm, making the $D/t$-ratio approximately 30 which is common in many offshore pipelines [21]. By using a portable ultra-sound measuring device, the average thickness of the pipe was measured to 3.89 mm. Further, the pipe's supports are two rigid cylinders of diameter 50 mm. Fig. 3 shows a sketch of the experimental setup. During testing, the contact force between the impactor and the pipe is sampled by a load cell [22]. Deformation of the pipe corresponds well with the three modes of deformation identified by Thomas et al. [6]: crumpling, crumpling and bending, and finally structural collapse. This experimental setup is replicated numerically in the following section.

## 4 NUMERICAL SIMULATIONS

### 4.1 General setup

All simulations have been carried out in the explicit finite element code Europlexus [23]. Four main cases have been defined for the numerical simulations, these being impact against pipes in various settings, the differences among which will be examined.

0. Pipes in air, with no internal pressure as in Fig. 3
1. Pipes in air, with internal pressure of 10 MPa (100 bar)
2. Pipes submerged in water, with no internal pressure
3. Pipes submerged in water, with internal pressure of 10 MPa (100 bar)

### 4.2 Spatial discretisation

The pipe is discretised using 4-node Lagrangian shell elements called `Q4GS`, with 6 degrees of freedom per node and 20 Gauss points in total (5 across the thickness). Three

mesh grades for the pipe are used (number of elements, circumference × length): coarse (16×52), medium (24×78) and fine (32×104). A fluid mesh immerses the pipe in cases 2 and 3, and the mesh is completely Eulerian and discretised by 8-node linear bricks with 1 Gauss point per element (type `CUBE` in Europlexus), whose size is slightly smaller than those of the structure. The fluid mesh measures 0.3 m × 0.5 m × 1.5 m and has an absorbing boundary to avoid wave reflections, and the pipe is located off centre so it can deform within the fluid boundaries.

40 spherical material points represent the rigid impactor and supports, thus approximating a cylinder. The supports are fixed in space, while the impactor is given an initial velocity of 3.24 m/s (other velocities were also investigated). Contact is enforced by the "pinball" model [24], with a fixed diameter of 20 mm for the impactor and 50 mm for the supports. The contact sections of the pipe have "hierarchic" pinballs with an initial diameter of the order of the shell's length. This initial diameter is then recursively reduced to the order of the shell's thickness, allowing finer spatial resolution of the contact conditions.

### 4.3 Fluid-structure interaction

The fluid is modeled by the Euler equations, describing conservation of mass, momentum and energy [25]. A crucial part of the simulations is how the fluid-structure interaction (FSI) is handled. As indicated, the Lagrangian structure is embedded in a Eulerian mesh. By using an embedded algorithm, the need for mesh rezoning techniques is effectively eliminated, albeit at the cost of some accuracy. This can be a difficult task, especially if the structure undergoes large rotations. To determine which fluid nodes that participate in the FSI, a sphere with a given radius[1] is placed on each structural node. The spheres are then connected via prisms, cones and hexahedra, creating a certain volume around the structure. This volume is called the *influence domain*, illustrated in 2D in Fig. 4(a). All fluid nodes within the influence domain participate in the FSI. As the calculation progresses and the structure deforms this domain has to be updated. The impactor has been left out of the FSI scheme, as it only serves as a vessel for delivering the kinetic energy to the pipe.

The FSI algorithm employed in this study is called the `FLSR` algorithm in Europlexus. It puts a certain restriction on the fluid velocity in each fluid node within the influence domain. A fluid node $F$ inside the domain (see Fig. 4(b)), located between structural nodes $S_1$ and $S_2$, is assigned a restriction: the fluid's velocity at this node, $\mathbf{v}_F$, along the structure normal $\mathbf{n}_S$, is set by a Lagrange multipliers method (see [25, 26]) to be equal to the structure's normal velocity $\mathbf{v}_{S^*}$ at the closest point $S^*$, i.e.

$$\mathbf{v}_F \cdot \mathbf{n}_S = \mathbf{v}_{S^*} \cdot \mathbf{n}_S = (N_1 \mathbf{v}_{S_1} + N_2 \mathbf{v}_{S_2}) \cdot \mathbf{n}_S \tag{7}$$

in which $N_1$ and $N_2$ are the shape functions. This attempts to leave the fluid free to slide along the structure, while it can not pass through the structure. Another alternative

[1] The radius should be large enough to include some fluid nodes, but not too many.

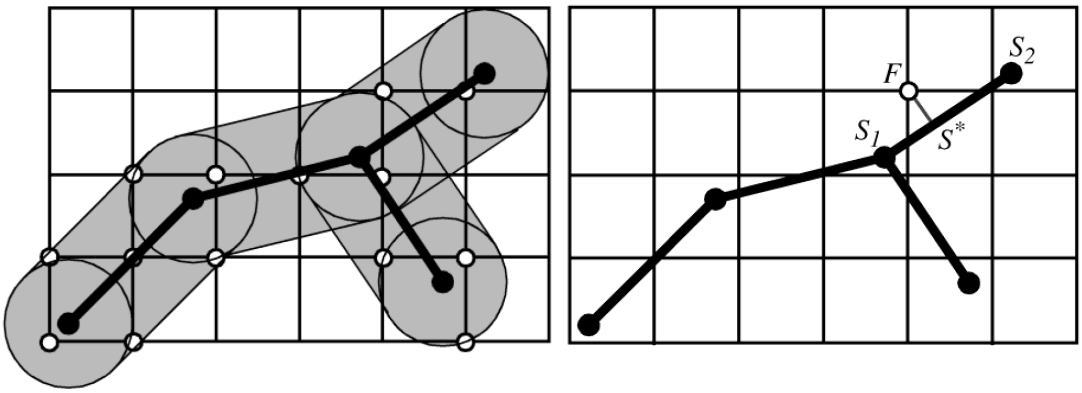


(a) Influence domain (shaded) (b) Fluid-structure coupling

**Figure 4**: Enforcement of fluid-structure interaction [26].

would be to tie the fluid velocity to the structural velocity in all spatial directions, i.e.

$$\mathbf{v}_F = \mathbf{v}_{S^*} = N_1 \mathbf{v}_{S_1} + N_2 \mathbf{v}_{S_2} \tag{8}$$

This has the advantage of hindering potential numerical fluid leakage, while it may cause some unphysical loading of the structure as it is a strong condition to impose. In Eq. (7), the fluid-structure coupling parameter (FSCP) is equal to 0, while in Eq. (8) it is 1.

### 4.4 Results

Results are mainly presented as the contact force between the pipe and the indenter plotted against the global transverse deformation/displacement of the pipe. First the empty pipe was simulated with different element sizes to check the mesh sensitivity. From Fig. 5(a) it is seen that the coarse mesh overestimates the peak force and thereby underestimates the final deformation. Both the medium and the fine mesh capture both the peak force and the deformation well. The medium mesh appears to be the best in terms of accuracy and computational cost, and further plots will have this discretisation of the structure. The simulation with this mesh, without pressure and without water and with an impact velocity of 3.24 m/s and thickness of 3.89 mm, will henceforth be referred to as the "reference simulation", i.e. the simulation of the actual experiment (case 0).

As the thickness of the pipe used in the experiment was not uniform, the effect of altering the shell thickness was investigated. By increasing the thickness, one would expect a slightly higher peak force and correspondingly lower final deformation. Fig. 5(b) shows that this is exactly the case, even with thickness variations of the order of hundredths of millimeters.

Inclusion of pressure (case 1) seems to lead to an increased peak force during the initial crumpling, and a lower force during the bending phase (see Fig. 6(a)). Total global deformation seems to be quite similar. The local deformation, however, is rather different.

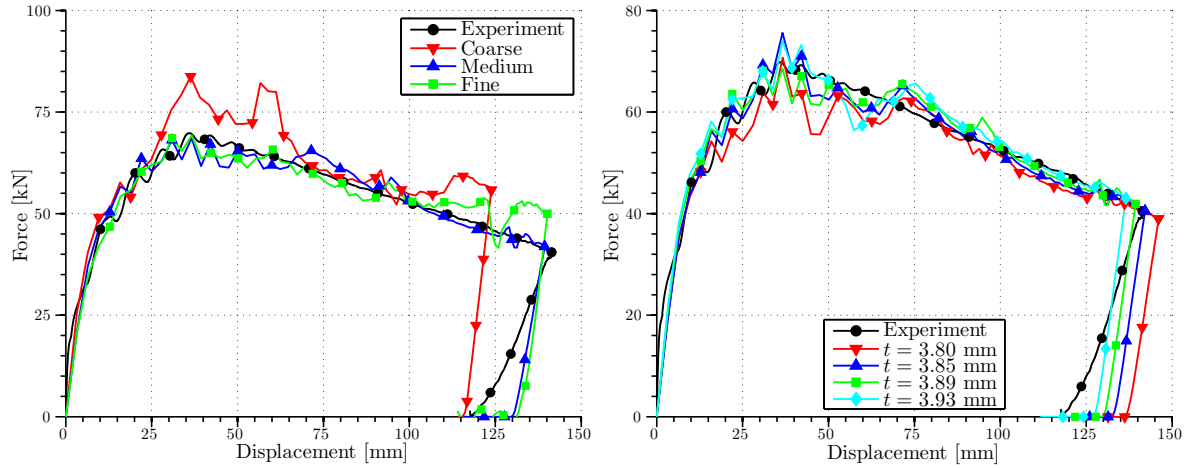


(a) Mesh sensitivity, $t = 3.89$ mm (b) Thickness variations, medium mesh

**Figure 5**: Effect of various parameters at $v_0 = 3.24$ m/s.

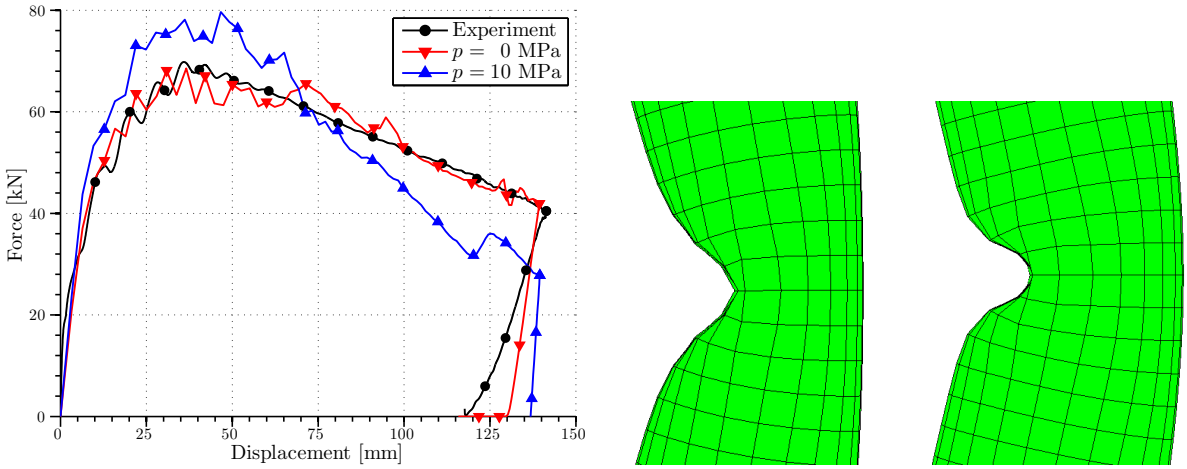


(a) Force-displacement (b) $p = 0$ MPa (c) $p = 10$ MPa

**Figure 6**: Medium mesh, $t = 3.89$ mm, showing the effect of including pressure (case 1).

It is observed that the curvature is steeper when including pressure, and that the pipe's cross-section at midpoint is less deformed (compare Figs. 6(b) and (c)). This is observed experimentally by Jones and Birch [10].

Simulations of case 2 show that the effect of the surrounding water depends heavily on how the FSI is enforced. Fig. 7(a) shows that when only the normal velocities are involved, there is almost no difference compared to the reference simulation. Tying the fluid velocity to the structure velocity in all directions increases the peak force, causing a comparatively lower deformation, and a seemingly incorrect solution. The same observations apply to case 3, where also internal pressure is included (see Fig. 7(b)).

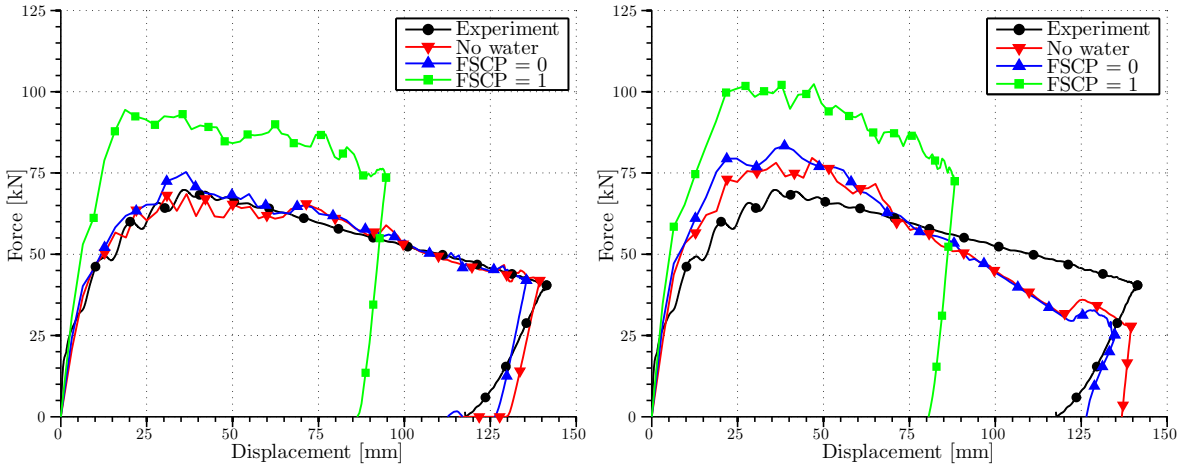


(a) Effect of water (case 2) (b) Effect of water and pressure (case 3)

**Figure 7**: Medium mesh, $t = 3.89$ mm.

Additional simulations have been carried out to investigate the potential effect of increasing the impact velocity while retaining the amount of kinetic energy delivered to the system constant. Results from these simulations are shown in Fig. 8(a), which shows that increasing the velocity to 10 m/s has virtually no effect and the solution is almost identical to the reference simulation. A higher amplitude of the oscillations are obtained when increasing to 20 m/s, and at 30 m/s a distinct difference is observed with a rough doubling of the peak load. Running case 2 at 10 m/s produces a more evident effect of the surrounding water, although not particularly significant (compare Figs. 7(a) and 8(b)).

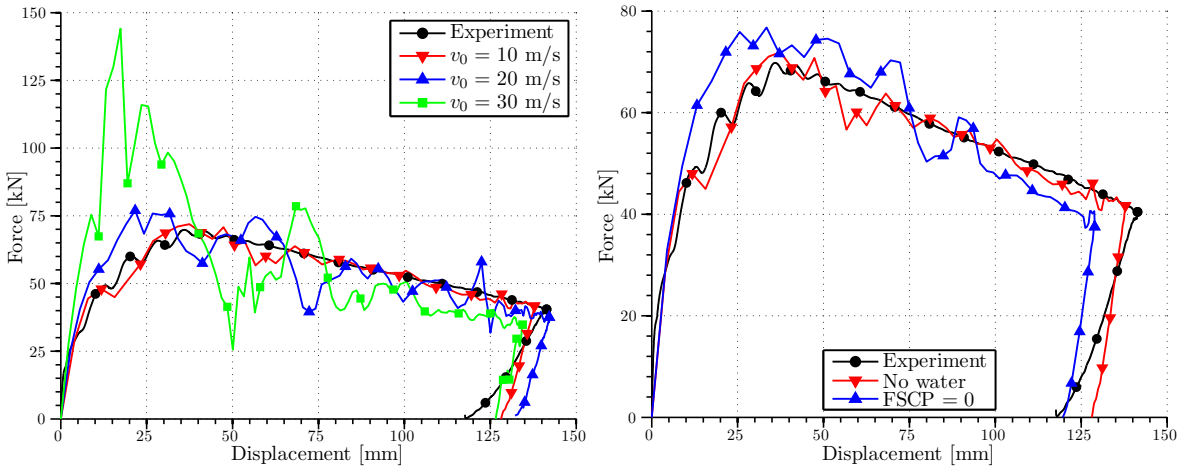


(a) Effect of velocity (b) Effect of water at $v_0 = 10$ m/s

**Figure 8**: Medium mesh, $t = 3.89$ mm.

## 5 DISCUSSION AND CONCLUDING REMARKS

Simulation results of case 0 show that Europlexus is capable of capturing the force-displacement curve from the impact experiments very well. In case 1 which includes internal pressure, a higher peak force was attained while the deformation was more localised and the pipe's cross-section at midspan was less deformed. This makes sense as the internal pressure acts normal to the pipe wall and thereby oppositely to any deformation of the cross-section. Global deformation was quite similar as the force during the end of the impact dropped compared to case 0. The amount of energy absorbed is still the same, but it is absorbed differently.

The effect of adding water depended greatly on how the FSI was enforced. Imposing equal velocity on the fluid as on the structure caused a large deviation from the other simulations and the experiment, thus indicating that such a choice is most likely not physical. Imposing equal *normal* velocity seemed to have very little effect on force level, local deformation and global deformation. Considering the immense increase in CPU cost by adding the water, omitting this effect seems for design purposes justified at low impact velocities. Similar tendencies were observed for case 3, where both water and internal pressure were considered. The mass of the impactor is large compared to the pipe and the water, which can be a contributing factor to why the water had such a small effect.

Finally, a short investigation of impact velocity was conducted. As the material is sensitive to strain rate, an increase in force was both expected and observed. Case 0 showed no significant difference at 10 m/s, while bigger oscillations were observed at 20 m/s. The peak load was roughly doubled at 30 m/s. Where virtually no effect of immersing the pipe in water was found at 3.24 m/s, tendencies to higher peak load and lower global deformation were observed at 10 m/s – this is expected as the drag forces are proportional to the velocity. However, for the velocities envisaged in the guidelines given by DNV, water may, as mentioned, for practical purposes be neglected.

## REFERENCES

[1] N. Jones. Inelastic response of structures due to large impact and blast loadings. *Journal of Strain Analysis for Engineering Design*, 45:451–464, 2010.

[2] Statoil ASA. *Small gas leak from Kvitebjørn pipeline*, Cited 23.01.2013. `http://www.statoil.com/en/NewsAndMedia/News/2008/Pages/gasleakkvitebjorn.aspx`.

[3] N. Jones and R.S. Birch. Influence of internal pressure on the impact behaviour of steel pipelines. *International Journal of Pressure Vessel Technology*, 118:464–471, 1996.

[4] DNV. *Offshore standard DNV-OS-F101: Submarine pipeline systems*. Det Norske Veritas, 2008.

[5] DNV. *Offshore standard DNV-RP-F111: Interference between trawl gear and pipelines*. Det Norske Veritas, 2010.

[6] S.G. Thomas, S.R. Reid, and W. Johnson. Large deformations of thin-walled circular tubes under transverse loading – I: An experimental survey of the bending of simply supported tubes under a central load. *International Journal of Mechanical Science*, 18:325–333, 1976.

[7] N. Jones, S.E. Birch, R.S. Birch, L. Zhu, and M. Brown. An experimental study on the lateral impact of fully clamped mild steel pipes. *Proceedings of IMechE, Part E: Journal of Process Mechanical Engineering*, pages 111–127, 1992.

[8] W.Q. Shen and D.W. Shu. A theoretical analysis on the failure of unpressurised and pressurised pipelines. *Proceedings of the Institution of Mechanical Engineers 216 (E)*, pages 151–165, 2002.

[9] C.S. Ng and W.Q. Shen. Effect of lateral impact loads on failure of pressurised pipelines supported by foundation. *Proceedings of the Institution of Mechanical Engineers 220 (E)*, pages 193–206, 2006.

[10] N. Jones and R.S. Birch. Low-velocity impact of pressurised pipelines. *International Journal of Impact Engineering*, 37:207–219, 2010.

[11] M. Kristoffersen, T. Børvik, I. Westermann, M. Langseth, and O.S. Hopperstad. Impact against X65 steel pipes — an experimental investigation. *Submitted for possible journal publication*, 2013.

[12] C.-K. Oh, Y.-J. Kim, J.-H. Baek, and W.-S. Kim. Development of stress-modified fracture strain for ductile failure of API X65 steel. *International Journal of Fracture*, 143:119–133, 2007.

[13] M. Kristoffersen, T. Børvik, M. Langseth, H. Ilstad, E. Levold, and O.S. Hopperstad. Damage and failure in an X65 steel pipeline cause by trawl gear impact. *Proceedings of the ASME 2013 32$^{nd}$ International Conference on Ocean, Offshore and Arctic Engineering*, 2013.

[14] Y. Chen, A.H. Clausen, O.S. Hopperstad, and M. Langseth. Application of a split-Hopkinson tension bar in a mutual assessment of experimental tests and numerical predictions. *International Journal of Impact Engineering*, 38:824–836, 2011.

[15] G.R. Johnson and W.H. Cook. A constitutive model and data for metals subjected to large strains, high strain rates and high temperatures. *Proceedings of the 7$^{th}$ International Symposium on Ballistics*, pages 541–547, 1983.

[16] B. Moras. Constitutive Equations of Strain Rate Sensitive Metals for the Automotive Industry. Technical report, Structural Mechanics Unit, Joint Research Centre, Ispra, Italy, 1999.

[17] R. Hill. *The Mathematical Theory of Plasticity*. Oxford University Press, 1950.

[18] G. Le Roy, J.D. Embury, and M.F. Ashby. A model of ductile fracture based on the nucleation and growth of voids. *Acta Metallurgica*, 29:1509–1522, 1981.

[19] K. Slåttedalen and A. Ørmen. Impact against offshore pipelines – Experiments and numerical simulations. Master's thesis, Norwegian University of Science and Technology, 2010.

[20] A.G. Hanssen, T. Auestad, T. Tryland, and M. Langseth. The kicking machine: A device for impact testing of structural components. *International Journal of Crashworthiness*, 8:385–392, 2003.

[21] A. Manes, R. Porcaro, H. Ilstad, E. Levold, M. Langseth, and T. Børvik. The behaviour of an offshore steel pipeline material subjected to stretching and bending. *Ships and Offshore Structures*, 7:371–387, 2012.

[22] A.G. Hanssen, T. Auestad, M. Langseth, and T. Tryland. Development of a 3-component load cell for structural impact testing. *International Journal of Mechanics and Materials in Design*, 2:15–22, 2005.

[23] Joint Research Centre. *Europlexus user's manual*, Cited 16.03.2012. `http://europlexus.jrc.ec.europa.eu/public/manual_pdf/manual.pdf`.

[24] T. Belytschko and M.O. Neal. Contact-impact with the pinball algorithm with penalty and Lagrangian methods. *International Journal for Numerical Methods in Engineering*, 31:547–572, 1991.

[25] F. Casadei and N. Leconte. Coupling finite elements and finite volumes by Lagrange multipliers for explicit dynamic fluid-structure interaction. *International Journal for Numerical Methods in Engineering*, 86:1–17, 2011.

[26] F. Casadei, M. Larcher, and N. Leconte. Strong and weak forms of a fully non-conforming FSI algorithms in fast transient dynamics for blast loading of structures. *III ECCOMAS Thematic Conference on Computational Methods in Structural Dynamics and Earthquake Engineering, Corfu, Greece*, May 2011.